A Short-Pulse Indirect ToF Imager Using 6-Tap Pixel with Backside Illuminated Structure for High-Speed Charge Demodulation

Tomohiro Okuyama[1], Haruya Sugimura[1], Gabriel Alcade[1], Seiya Ageishi1, Hyeun Woo Kwen[1], De Xing Lioe[1,2], Kamel Mars[1, 3], Keita Yasutomi[1,2], Keiichiro Kagawa1, Shoji Kawahito[1,2]
1 Shizuoka University, Hamamatsu, 432-8011, Japan
2 SUiCTE Co. Ltd., Hamamatsu, 432-8011, Japan
3 Shizuoka Institute of Science and Technology, Fukuroi, 437-0032 Japan
E-mail: toku@idl.rie.shizuoka.ac.jp

***Abstract*— This paper presents a short-pulse indirect time-of-flight (SP iToF) sensor using 6-tap pixels with a backside illumination (BSI) structure. The sensor demonstrates a fast response to near infrared (NIR) light and achieves high depth linearity (<0.8%FS) and resolution (<2%) over a range of 3-28 meters indoors. A comparison between 6-tap iToF sensors with front-side illumination (FSI) and BSI structures exhibits that the BSI structure provides a faster response to NIR light. The SP iToF pixel contains a photodiode and a charge demodulator, with six gates (G1 to G6) and one drain (GD). The BSI sensor, with a 5 µm substrate, shows superior performance due to faster response times, which improves linearity and depth resolution. This paper presents detailed measurements of the iToF sensor response using a short pulse laser and shows that BSI sensors have significantly smaller time constants (τ_1 and τ_2 compared to FSI sensors. This improvement is attributed to the thinner substrate of the BSI sensor.**

Keywords—component, formatting, style, styling, insert *(key words)*

I. INTRODUCTION

There has been a significant shift in the design of indirect time-of-flight (iTOF) image sensors from front-side illumination (FSI) to backside illumination (BSI) [1-5]. This transition has been driven by the need to improve the signal-to-noise ratio (SNR) and increase the sensing performance of ToF sensors, particularly in outdoor environments where background light, such as sunlight, can introduce significant noise.

To mitigate the effects of background light noise, light sources with wavelengths of 940nm or longer, which are less affected by atmospheric absorption, are often used. However, conventional FSI image sensors suffer from reduced quantum efficiency (QE) at these longer wavelengths. Increasing the epitaxial layer thickness can improve sensitivity at longer wavelengths by extending the optical path length, but this also leads to a reduction in modulation contrast due to charge generation occurring further from the demodulation gate [6]. There is therefore a trade-off between QE and modulation contrast in FSI sensors [7, 8].

BSI image sensors, on the other hand, use reflective materials in the metal layer [9] and backside structures such as inverted pyramids [2, 10] and deep trench isolation (DTI) to achieve a longer optical path length to improve near-infrared (NIR) QE. As a result, BSI iTOF sensors do not face the same trade-off between NIR QE and modulation contrast as FSI sensors. The improvement in QE directly contributes to better range performance in iTOF sensors. In addition, the thinner substrate in BSI sensors improves modulation contrast, which further enhances range performance.

In this paper, we compare the modulation contrast of 6-tap iTOF image sensors fabricated using the FSI and BSI processes, based on the same pixel layout. We evaluate their responses to two types of pulsed light sources with full-width half-maximum (FWHM) of 15ns and 69ps. The BSI 6-tap iTOF sensor uses a short-pulse (SP) iTOF method. This method is advantageous for long distance measurements (over 10 meters) in outdoor environments because it uses the pulse light with a small duty cycle. This allows for higher peak power with lower average power, which reduces the effect of background light [5, 11]. The

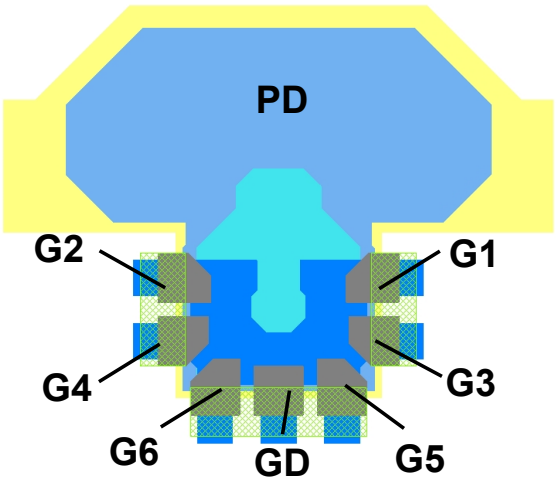

Fig. 1. 6-tap iToF pixel layout

sensor showed a linearity error of less than 0.8% full scale (FS) and a depth resolution of less than 2% over a distance range of 3-28 meters using two subframes.

II. The 6-tap SP-iToF Sensor and Operation

Figure 1 shows the layout of the photodiode and charge demodulator of the pixel, which is common to both the BSI and FSI iToF sensors. The sensors were fabricated using a 0.11 µm CMOS image sensor process. The number of pixels is 1080(H) x 488(V). The size of the pixel is 8.4 µm x 8.4 µm. The charge demodulators have 6 gates (G1 to G6) and 1 drain (GD). The photoelectrons generated in the photodiode are transferred to the demodulator by the electric drift field created by the impurity doping. They are further transferred to the respective floating diffusion for each time window by gating operations. The FSI uses 20 µm epi-wafers, and the BSI's substrate thickness is 5 µm. A back-substrate bias of −3V is used.

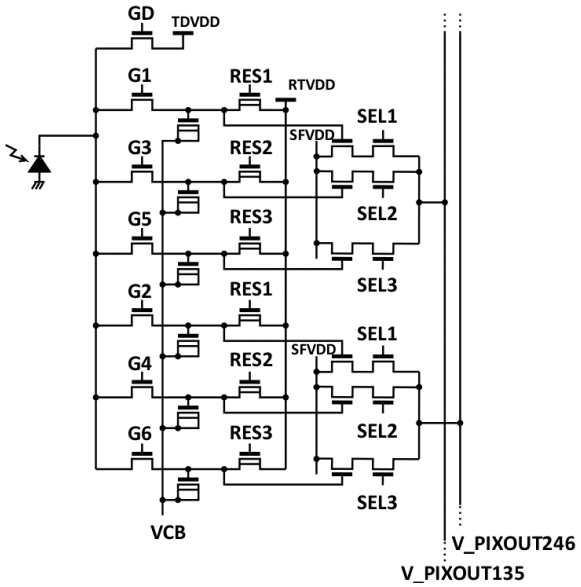

Fig. 2. 6-tap iToF pixel readout circuits

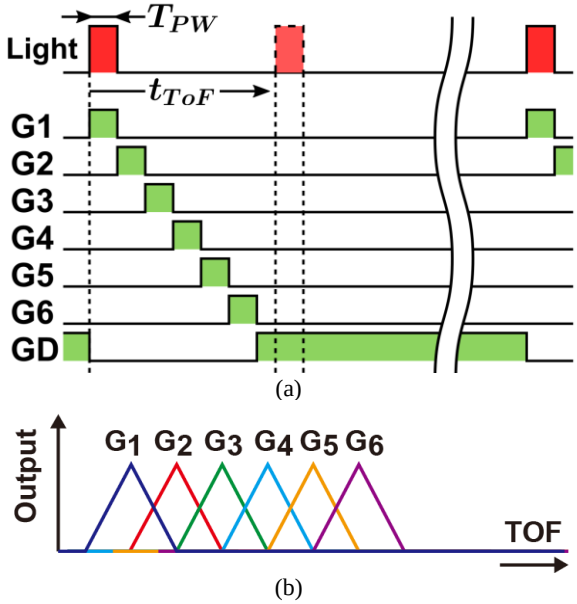

Fig. 3. 6-tap iToF pixel operation (a) Timing diagram for Gating (b) Required ToF response

Figure 2 shows the 6-tap iToF pixel circuit. The 6-tap demodulator operates with six short-pulse clocks corresponding to G1-G6 and a clock for the drain gate GD. The output signals from each tap are sequentially selected by the tap selection signals SEL1-3, with two taps being selected simultaneously. These signals are then output to the column readout circuit through two vertical lines.

Figure 3(a) illustrates the operation of the gates within the pixel. The short-pulse light source and the ToF pixels are synchronized, with the gates of the demodulator sequentially turning on from G1 to G6. After G6 turns off, GD turns on until G1 turns on in the next cycle, effectively draining the charge from background light.

Depending on the ToF, the signal output curve at each gate, shown in Figure 3(b), represents the ideal case. Ideally, the output at each tap varies linearly with the ToF. However, the response characteristics of the light source and demodulator can distort this behavior. This distortion affects the distance measurement performance.

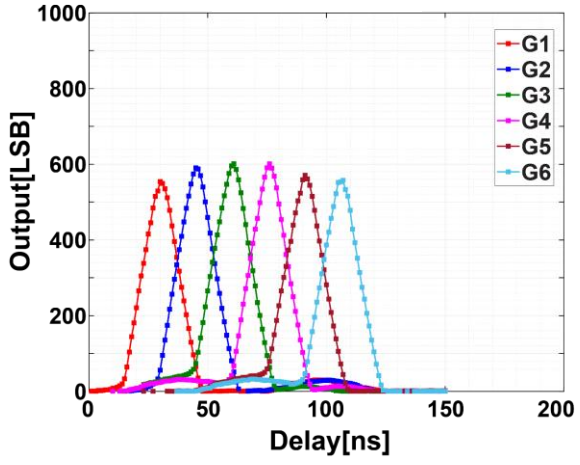

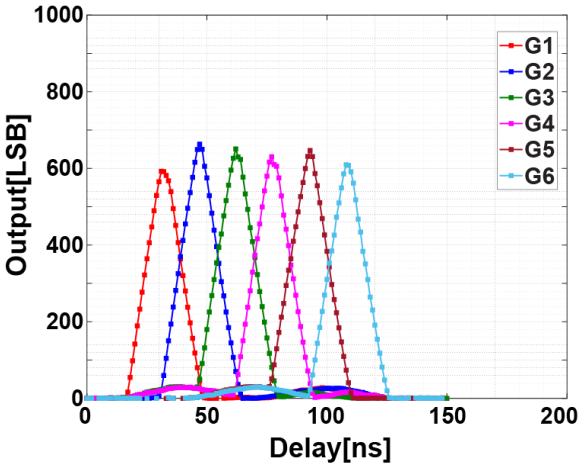

Fig. 4. Response to pulse delay (a) FSI (b) BSI

III. MEASUREMENT RESULTS

The output response curves of the 6-tap pixel when the timing of the incident pulsed light is delayed were measured as shown in Fig. 4. The measurements were conducted using a short-pulse light source with a pulse width of 15 ns, delayed by 1 ns increment using a delay controller. The light pulse period was 300 ns, and the wavelength was 940 nm. A bandpass filter with a center wavelength of 940 nm and a bandwidth of 10 nm was used. The output signal offsets were removed.

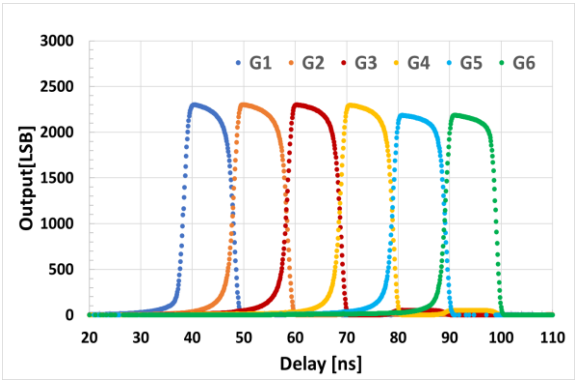

(a)

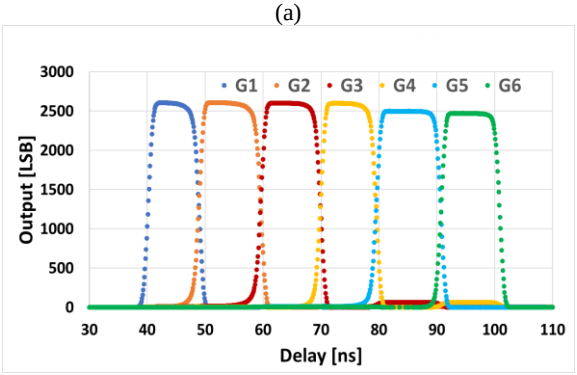

(b)

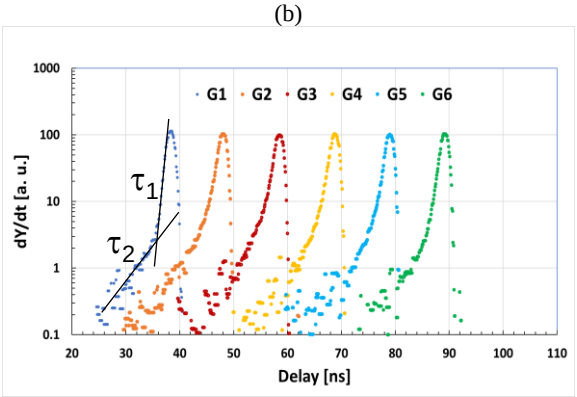

(c)

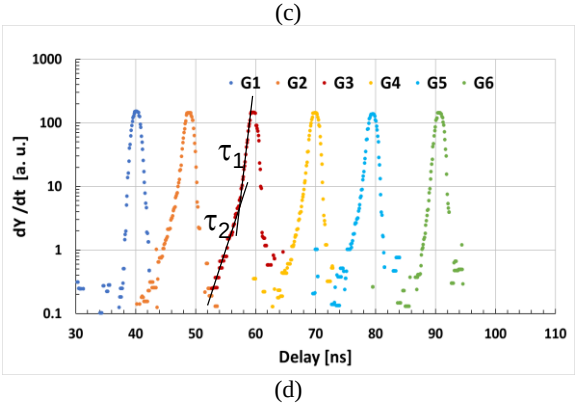

(d)

Fig. 5. Response to impulse delay (a) Impulse response of FSI output (b) Impulse response of BSI output (c) Time-derivative of FSI output (d) Time-derivative of BSI output

Figures 4(a) and 4(b) show the response curves to pulse delay for the FSI sensor and BSI sensor, respectively. The FSI sensors exhibit good characteristics, but the BSI sensors demonstrate even better and more symmetrical triangular characteristics, indicating superior modulation contrast and sensitivity.

To verify the detailed characteristics of the demodulator, the response of each gate output was measured using a very short-pulse light source. The iTOF pixel gates were driven with a 10 ns short-pulse clock, with a period of 300 ns. The short-pulse light source has a wavelength of 850 nm and FWHM of 69 ps. Figure 5 shows the sensor outputs for each gate: (a) for FSI and (b) for BSI. Their time derivatives are plotted in (c) and (d). Table 1 summarizes the time

Table 1. Time constants of 6-tap pixel response

Gate	FSI		BSI	
	τ_1 (ns)	τ_2 (ns)	τ_1 (ns)	τ_2 (ns)
G_1	0.48	2.42	0.35	0.21
G_2	1.08	3.09	0.52	1.14
G_3	1.13	3.99	0.53	1.08
G_4	1.04	2.52	0.48	0.84
G_5	0.98	2.73	0.45	0.88
G_6	0.85	2.72	0.40	0.58
Ave.	0.93	2.91	0.46	0.79

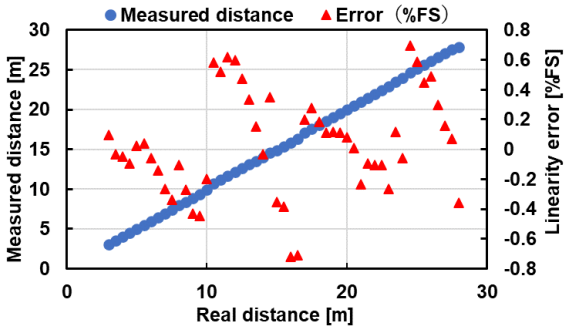

(a)

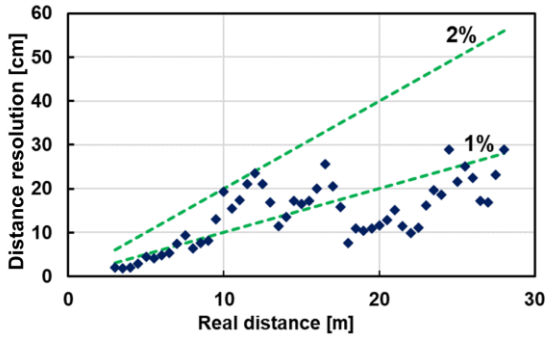

(b)

Fig. 6. Results of measured depth at indoor in the range 3-28 m (a) Measured linearity and distance error (b) Distance resolution

(a)

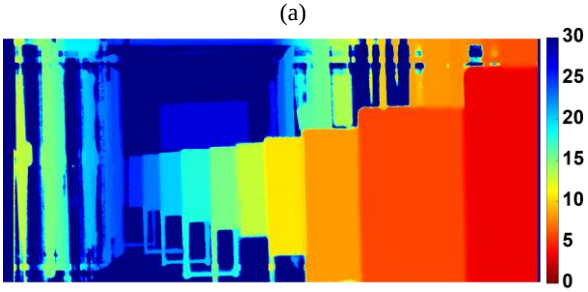

(b)

Fig. 7. Distance image: (a) Environment setup (b) Captured depth image

constants τ_1 and τ_2 for both FSI and BSI. In BSI, τ_1 and τ_2 are 2 and 3 times smaller, respectively, compared to FSI. This is due to the thinner epitaxial layer in BSI sensors, which increases the proportion of electrons that can be transferred quickly. As a result, BSI sensors achieve more efficient demodulation and faster response times.

The distance measurement was demonstrated using the BSI SP iToF sensor over a range of 3–28 m in an indoor environment. Light pulses and gate driving clocks both has a pulse width of 15 ns, with two subframes used to extend the measurement range [3]. Figure 5(a) shows the linearity and error of the BSI SP iToF sensor measured indoors, and (b) shows the distance resolution. At the distance of 28 m, the sensor achieved a linearity error of <0.8%FS and a depth resolution of <2%. Figure 6 shows a distance image taken with the implemented ToF camera.

CONCLUSION

The SP iToF sensor with BSI structure shows better performance than the FSI sensor. The BSI sensor's thinner substrate and quick response to near-infrared light result in smaller time constants (τ_1 and τ_2), improving depth linearity and resolution. Additionally, the BSI structure not only provides optical advantages but also significantly enhances the speed of charge modulation. This makes the BSI sensor ideal for precise depth sensing indoors over 3–28 meters. Future work will focus on optimizing the pixel structure specifically for BSI, which is expected to further improve the sensor's characteristics.

ACKOWLEDGMENTS

This work was supported in part by the JSPS KAKENHI Grant Number 24H00313. The authors would like to thank Mr. Y. Ohkubo and Mr. T. Nakagome of TOPPAN Holdings, Inc. for helpful discussion. The authors appreciate DB HiTek for chip fabrication.

REFERENCES

[1] Y. Kato et al., " 320 × 240 back-illuminated 10- μ m CAPD pixels for high-speed modulation time-of-flight CMOS image sensor ", *IEEE J. Solid-State Circuits*, vol. 53, no. 4, pp. 1071-1078, Apr. 2018.

[2] Y. Ebiko et al., "Low power consumption and high resolution 1280×960 gate assisted photonic demodulator pixel for indirect time of flight", *IEDM Tech. Dig.*, pp. 33, Dec. 2020.

[3] Y. Kwon et al., " A 2.8 μ m pixel for time of flight CMOS image sensor with 20 ke-full-well capacity in a tap and 36% quantum efficiency at 940 nm wavelength ", *IEDM Tech. Dig.*, pp. 33, Dec. 2020.

[4] M.-S. Keel et al., " A 4-tap 3.5 μ m 1.2 Mpixel indirect time-of-flight CMOS image sensor with peak current mitigation and multi-user interference cancellation ", *IEEE ISSCC Dig. Tech. Papers*, pp. 106-108, Feb. 2021.

[5] K. Hatakeyama *et al*., "A Hybrid ToF Image Sensor for Long-Range 3D Depth Measurement Under High Ambient Light Conditions," in *IEEE Journal of Solid-State Circuits*, vol. 58, no. 4, pp. 983-992, April 2023.

[6] C. S. Bamji et al., "A Review of Indirect Time-of-Flight Technologies," in *IEEE Transactions on Electron Devices*, vol. 69, no. 6, pp. 2779-2793, June 2022.

[7] C. S. Bamji et al., " A 0.13 μ m CMOS system-on-chip for a 512 × 424 time-of-flight image sensor with multi-frequency photo-demodulation up to 130 MHz and 2 GS/s ADC ", *IEEE J. Solid-State Circuits*, vol. 50, no. 1, pp. 303-319, Jan. 2015.

[8] F. Acerbi et al., "Optimization of pinned photodiode pixels for high-speed time of flight applications", *IEEE J. Electron Devices Soc.*, vol. 6, pp. 365-375, 2018.

[9] M. S. Oh et al., " Backside-illumination 14 μ m-pixel QVGA time-of-flight CMOS imager ", *Proc. 10th IEEE Int. NEWCAS Conf.*, pp. 325-328, Jun. 2012.

[10] I. Oshiyama et al., "Near-infrared sensitivity enhancement of a back-illuminated complementary metal oxide semiconductor image sensor with a pyramid surface for diffraction structure," *2017 IEEE International Electron Devices Meeting (IEDM)*, San Francisco, CA, USA, 2017, pp. 16.4.1-16.4.4

[11] S. Kawahito, K. Yasutomi and K. Mars, "Hybrid Time-of-Flight Image Sensors for Middle-Range Outdoor Applications," in *IEEE Open Journal of the Solid-State Circuits Society*, vol. 2, pp. 38-49, 2022.